

# **Biomimetic topography and chemistry control cell attachment to amyloid fibrils**

*Nicholas P. Reynolds<sup>1,2\*</sup>, Mirren Charnley<sup>2,3</sup>, Marie N. Bongiovanni<sup>4,5,6</sup>, Patrick G. Hartley<sup>7</sup>,  
Sally L. Gras<sup>5,6\*</sup>*

<sup>1</sup> Manufacturing Flagship, CSIRO, Bayview Avenue, Clayton, Victoria 3169, Australia

<sup>2</sup> ARC Training Centre for Biodevices, Faculty of Science, Engineering and Technology,  
Swinburne University of Technology, Victoria, 3122, Australia

<sup>2</sup> Centre for Micro-Photonics, Faculty of Science, Engineering and Technology, Swinburne  
University of Technology, Victoria, 3122, Australia

<sup>3</sup> Industrial Research Institute Swinburne, Faculty of Science, Engineering and Technology,  
Swinburne University of Technology, Victoria, 3122, Australia

<sup>4</sup> Department of Chemistry, University of Cambridge, Cambridge, CB2 1EW, United Kingdom

<sup>5</sup> The ARC Dairy Innovation Hub, Department of Chemical and Biomolecular Engineering, The  
University of Melbourne, Parkville Victoria, 3010, Australia

<sup>6</sup> The Bio21 Molecular Science and Biotechnology Institute, The University of Melbourne,  
Parkville VIC 3010, Australia

<sup>7</sup> Energy Flagship, CSIRO, Private Bag 10, Bayview Avenue, Clayton, Victoria 3169, Australia

Key Words: Amyloid Fibril, Self-assembling Peptides, Biomaterials, Transthyretin, TTR, Plasma Polymer, Nanoscale Topography, Biomimetic Chemistry

## **Abstract**

Networks of nanoscale fibrous coatings made from self-assembled peptides are promising candidates for biomaterials that can promote the growth of mammalian cells. One particularly attractive feature is the possibility of adding bio-functional sequences to peptides to promote cell attachment. We deconvolute the topographic and chemical effects of nanoscale fibrils on cells by depositing a plasma polymer film on TTR1-based fibrils decorated with a range of cell adhesive chemistries (RGD and cycloRGDfK), producing a surface that retains the nanoscale fibrous topography of surface bound fibrils but lacks the fibril surface chemistry. The surface topography was found to influence cell toxicity and spreading and the fibril surface chemistry influenced cell attachment and spreading. This study highlights the importance of considering both the chemical and physical features of novel biomaterials and illustrates the use of plasma polymer deposition as a tool for examining the relationship between amyloid fibril structure and function.

## **Introduction**

Amyloid fibrils assembled either from synthetic peptides<sup>1-3</sup> or globular proteins<sup>4-6</sup> are emerging as potential scaffolds and biomaterials<sup>1,4,7</sup> for the growth of mammalian cells. Fibrils may also be combined with materials such as graphene,<sup>6</sup> DNA<sup>8</sup> or plasma polymers<sup>5</sup> to form biomimetic hybrids with a broader range of properties. Recent interest in amyloid fibrils as functional biomaterials has arisen due to a number of factors. First, there is increasing evidence that mature

amyloid fibrils may be inert with soluble pre-fibrillar aggregates<sup>9-12</sup> or even the aggregation process<sup>13</sup> causing toxicity in neurodegenerative diseases. Second, functional amyloid fibrils with beneficial physiological functions have been discovered, such as melanin storage in humans and biofilm formation in bacteria.<sup>14</sup> Third, amyloid fibrils can be designed to display topographic and chemical properties that mimic properties of typical human cellular microenvironment, including the extracellular matrix (ECM), encouraging cell adhesion.<sup>1,4</sup>

The ECM is a dense network of nanoscale fibrous proteins and associated biomolecules that determines cell function in the majority of mammalian cellular microenvironments.<sup>15</sup> Biomimicry of the ECM is an important requirement for new biomaterials that attempt to promote or control physiological cellular responses<sup>16</sup> and can be used to promote the adhesion of cells.<sup>5,17,18</sup> Both the surface topography and chemistry should be carefully considered when rationally designing new biomaterials that aim to mimic the ECM.

The importance of material topography was previously shown by Reynolds *et. al.* who found cell attachment and spreading increased on plasma polymer films possessing a nanoscale topography that mimicked the ECM.<sup>5</sup> Luna *et. al.* used biomimetic nanotopography to align neonatal and embryonic stem cell derived cardiomyocytes, simulating the complex anisotropic, multi-scale architecture of the heart<sup>17</sup> and Wang *et. al.* used a soft lithographic technique to develop a series of PDMS pillars to mimic the morphology of the inner surface of the intestine, demonstrating that the topography affected the spreading, differentiation and metabolic activity of an intestinal epithelial -like cell line.<sup>18</sup>

Chemical cues can also be used to promote cell adhesion to nanoscale fibrous biomaterials, typically through the addition of short peptide sequences identified from the ECM to the surface of the fibrils or other fibrous assemblies.<sup>1,3</sup> *In vivo* these sequences decorate the surface of fibrous proteins that compose the majority of the ECM and mediate cellular adhesions between the cell membrane and the ECM.<sup>19</sup> Examples include the RGD tri-peptide sequence from fibronectin or the IKVAV sequence from laminin.

Here, we investigate the relative effects of surface topography and chemistry for a range of nanoscale amyloid fibrils fabricated from short synthetic peptides. The peptides chosen were fragments from the amyloid forming protein transthyretin (TTR), which form fibrils characterized from the atomic length-scale upwards.<sup>11,19-21</sup> We compare fibrils assembled from the un-functionalized TTR<sub>105-115</sub> fragment (TTR1) with TTR1-RGD and TTR1-cycloRGDfK (TTR1-cRGD) fibrils, where the RGD group is positioned at the C-terminus of the peptide. These modified peptides retain the ability to assemble fibrils with the same core structure where RGD is present on the surface of the fibril<sup>21-23</sup> and can promote cell adhesion.<sup>1</sup>

Separating the effects of topography and surface chemistry for TTR1-based fibrils is non-trivial, as the topography of the assembled fibrils is dependent on peptide sequence despite the fibril core remaining identical.<sup>1,21</sup> We overcome this problem by depositing plasma polymer films generated from the monomer diglyme (DGpp)<sup>24-26</sup> on the networks of amyloid fibrils adsorbed to solid surfaces. Such an approach has previously been shown to replicate the nanoscale

topography of amyloid fibril coatings with extremely high fidelity whilst completely masking the surface chemistry of the underlying fibril, due to the thickness of the film (approx. 150 nm).<sup>5</sup>

The interaction between TTR1-based fibrils and cells appears complex and the differences between these designed fibrils and functional fibrils unclear. While cells interact favorably with TTR1-based functionalized fibrils over short time frames,<sup>1,27</sup> these fibrils compromise cells if incubated at the high concentrations typical of materials for extended periods of time, particularly when fibrils are coated on a surface.<sup>28</sup> The DGpp layer provides an opportunity to probe the topographic and chemical contributions to the toxicity of TTR1-based fibrils on a surface and could offer a route to a hybrid material that features of the topography of TTR1-based fibrils with the chemistry introduced by the DGpp layer.

By comparing attachment, spreading and viability of epithelial cells cultured on amyloid fibril coatings assembled from TTR1, TTR1-RGD and TTR1-cRGD peptides, both with and without the deposited DGpp layer we are able to elucidate the relative influences of biomimetic surface topography and chemistry in potential amyloid fibril biomaterial coatings.

## **Materials and Methods**

### **Peptide synthesis**

The peptide TTR1-cycloRGDfK was produced at the Bio21 Molecular Science and Biotechnology Institute (Melbourne, Australia). According to the methods published in

Bongiovanni *et. al.*<sup>1</sup> Briefly, the amino acid sequences YTIAALLSPYSC-NH<sub>2</sub> and cyclised RGDfK (cRGD) were independently synthesized by standard Solid-Phase Peptide Synthesis chemistry using a Liberty microwave peptide synthesizer (CEM Corporation, North Carolina, USA), and the two were covalently bonded via a 3-maleimidopropionic acid linker attached to the side chain of the lysine. Equimolar amounts of purified linear YTIAALLSPYSC-NH<sub>2</sub> and cyclic [RGDfK(Mal)] (Mal is maleimidopropionate) were dissolved in ammonium acetate buffer (pH 6.5, 50 mM) and the reaction followed by mass spectrometry. Within 15 min the peptides had quantitatively coupled together to form a stable thioether linkage. The reaction solution was immediately purified preparatively to yield the desired product with >95% purity. TTR1-RGD and TTR1 peptides were synthesized and purified to >95% by CS Bio Co. (California, USA) according to the sequences described in Gras *et. al.*<sup>27</sup>

### **Fibril formation**

Fibrils were assembled by re-suspending each TTR1-based peptide separately at 10 mg/ml with 10% (v/v) CH<sub>3</sub>CN in high purity Milli-Q water of resistivity 18 M Ωcm, incubating this solution at 37 °C for 24 h and maturing the solution at room temperature for 28 days. The conversion from free peptide to fibrils was assessed at > 90 % at 28 days maturity.<sup>1</sup> Thioflavin T (ThT) fluorescence was measured for TTR1-cycloRGDfK fibrils or freshly dissolved peptide in order to measure the extent of fibril assembly. Samples were prepared at a concentration of 2 mg/mL in 10 mM potassium phosphate and 150 mM NaCl, pH 7.0 containing 47 mM ThT. This preparation was incubated for 10 min before 200 mL of each sample was added to a black 96-well plate (Nalge Nunc International, NY, U.S.A.). The fluorescence intensity was measured

using a FLUOstar OPTIMA Microplate Reader (BMG Labtech, NC, U.S.A.) with an excitation and emission wavelength of 480 nm and 440 nm respectively.

### **Preparation of Amyloid Fibril Networks**

Aqueous solutions of fibrils were deposited on freshly cleaved mica ( $5 \mu\text{l}$ ,  $0.625 \text{ mgml}^{-1}$ ) in a laminar flow hood. The surfaces were left in the flow hood overnight to allow evaporation of the solvent. Freshly prepared surfaces were then either used for further experiments or the plasma polymer film deposited on top of the network.

### **Plasma Polymer Deposition**

Plasma polymer thin films were deposited onto the TTR1-based fibril networks via the radio frequency glow discharge (RFGD) of the monomer diethylene glycol dimethyl ether (DG; BDH, 99% purity) in a custom-built reactor.<sup>26</sup> The plasma reactor consisted of a cylindrical glass chamber (height of 35 cm and diameter of 17 cm) fitted with two capacitively coupled electrodes, spaced 10 cm apart. The top electrode ( $d = 9.5 \text{ cm}$ ) was connected to a RF power supply (125 kHz), while the bottom electrode ( $d = 14 \text{ cm}$ ) was grounded. A round-bottom flask containing the monomer diglyme was connected to the reactor chamber via a stainless steel line and the flow of the monomer vapors was controlled via a manual valve. Substrates were placed on the lower electrode and a rotary pump was used to evacuate the chamber. The DG monomer was degassed three times prior to deposition. The plasma was ignited at a starting monomer

pressure of 20 Pa, for treatment times of 180 s at a deposition power of 50 W. A schematic of the DGpp deposition process is shown in Figure 1.

### **Atomic Force Microscopy**

An Asylum Research MFP-3D atomic force microscope (Santa Barbara, CA, USA) was used to measure surface topography in tapping mode with ultra-sharp silicon nitride tips (NSC15 noncontact silicon cantilevers, MikroMasch, Spain). The tips used in this study had a typical force constant of 40 N/m and a resonant frequency of 320 kHz. Typical scan settings involved the use of an applied piezo deflection voltage of 0.7 V at a scan rate of 0.8 Hz. All images were processed (1st order flattening algorithm and roughness parameters) using Igor Pro software, at least 3 independent substrates were analyzed when calculating Rrms roughness parameters. Fibril widths were calculated from line scans of the AFM images using the Igor Pro software, to account for tip broadening effects measurements were taken at full width at half maximum intensity (FWHM) of the features in the line scan. Mean fibril widths are quoted as an average of 20 measured widths measured across at least 3 separate experiments and combined in a single average.

### **Cell Culture**

Samples were placed in the wells of a 24-well plate (Nunc®) and then sterilized by immersion in 2X Anti-Anti (Antimycotic-Antibiotic, GIBCO®) solution for at least 60 min. An MA-104 monkey epithelial cell line was cultured to 80 % confluence in media (DMEM + GlutaMAX-

ITM+ 1000 mg/L Glucose, GIBCO®), supplemented with 1% v/v Penicillin/Streptomycin and 10% v/v FBS (fetal bovine serum, SAFC Biosciences®) at 37 °C with 5 % CO<sub>2</sub>/air atmosphere to 80% confluence. Cells were harvested by trypsinization (2 mL Tryple™ Express, Invitrogen®) and then washed by dilution in 30 mL media followed by centrifugation (300 g for 5 min). Processed cells were counted, re-suspended in media (75,000 cells/ml) and then added to samples (0.6 ml, 25,000 cells/cm<sup>2</sup> of well area) and incubated overnight at 37 °C with 5 % CO<sub>2</sub>/air atmosphere. After culture, non-adherent cells were removed by rinsing the samples in fresh media.

### **Cell Viability Assay**

Cell viability of adhered cells after rinsing was investigated via esterase activity and membrane integrity using the LIVE/DEAD® assay (2 μM Calcein AM, 4 μM ethidium homodimer-1, Invitrogen®) solution in DPBS (Dulbecco's phosphate buffered saline, GIBCO®) for at least 20 minutes. Stained adhered cells were imaged on an inverted microscope (Nikon Eclipse TE2000-U, 10x objective lens). Images were captured sequentially with calcein excited at 465-495 nm and the resulting emission observed between 515-555 nm. Ethidium homodimer-1 was excited at 510-560 nm and the resulting emission observed above 590 nm.

### **Immunofluorescence Assays**

Cells were cultured on the different fibril and plasma polymer treated surfaces for 18 h before fixing in paraformaldehyde 4% (w/v) in DPBS, for 15 min and permeabilized by the addition of

Triton X-100 (0.1% (v/v) in DPBS, 10 min, Fluka). Samples were blocked in bovine serum albumin (BSA; 1% (w/v) in DPBS, Sigma-Aldrich) for 30 min. Samples were rinsed and incubated with the primary antibody for the focal adhesion (FA) protein vinculin (1: 200 dilution in 1% BSA) for 60 min, rinsed and subsequently incubated with Alexa Fluor 568 goat antimouse IgG (1:500 dilution, in 1% BSA Molecular Probes) and Alexa Fluor-488 conjugated Phalloidin (1:20 dilution), for 60 min before a final rinse in DPBS, and imaged using an Olympus IX71 microscope (Olympus) and 100x objective lens (1.4NA Oil Plan Apochromat).

### **Statistical analysis**

Statistical analysis of the average number of cells and cell spread area was performed over three separate experiments with three replicates and within each replicate three images were taken in non-overlapping regions. Average values were created for each experiment, and the final values presented as a mean of the three experiments. The results are reported as attached counts normalized to a mica control surface included in each experimental repeat. The number of viable cells was quantified using the image j program. Briefly images were converted to 8 bit black and white images, a threshold applied to improve contrast and the cells counted using the particle analysis tool; a method found to be within 5 % of the value calculated by hand. The spread area of cells was quantified from images recorded with the  $\times 10$  lens using the wand (tracing) tool and measure function in image j. A line bisecting the image was randomly drawn and the first 10 cells along that line were measured in each image. Statistical comparisons between the different functionalized substrates (eg, TTR1 vs TTR1-RGD or TTR1-RGD-DGpp vs TTR1-cRGD-DGpp) of both cell numbers and cell spreading area across the three experiments was performed using a students unpaired two way t-test using Minitab statistical software.

## Results

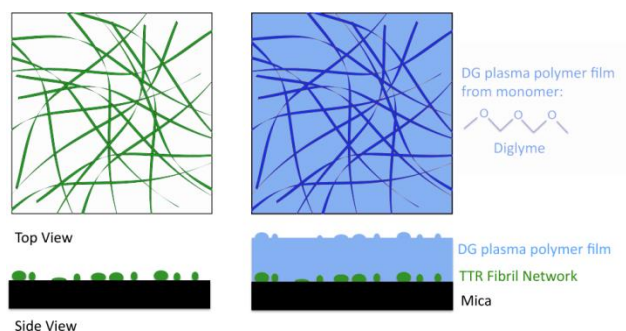


Figure 1: Schematic of the process of plasma polymer deposition on the fibril film.

### Characterization of Fibrous Nano-topography

Atomic Force Microscopy (AFM) was used to characterize the nanoscale topography of the three TTR1-based fibril coated mica surfaces, both before and after the deposition of the DGpp film (Figure 2). A concentration of fibrils was chosen ( $0.625 \text{ mgml}^{-1}$ ), to give an even surface coverage yet also allow individual fibrils to be resolved by AFM, see Figure S1 (supporting information) for AFM images at a range of fibril concentrations ( $2.5 - 0.16 \text{ mgml}^{-1}$ ). Previous studies have indicated that these<sup>19</sup> and other fibrils<sup>4</sup> have similar morphologies in solution or in a partially hydrated state, thus all AFM images were performed on partially hydrated samples in air. The nanoscale topography of all three surfaces was qualitatively similar both before and after the deposition of the DGpp layer. Furthermore, no significant change to the surface topography was observed after hydration of the DGpp films (in cell culture media for 18 h) (Figure 2 and S2).

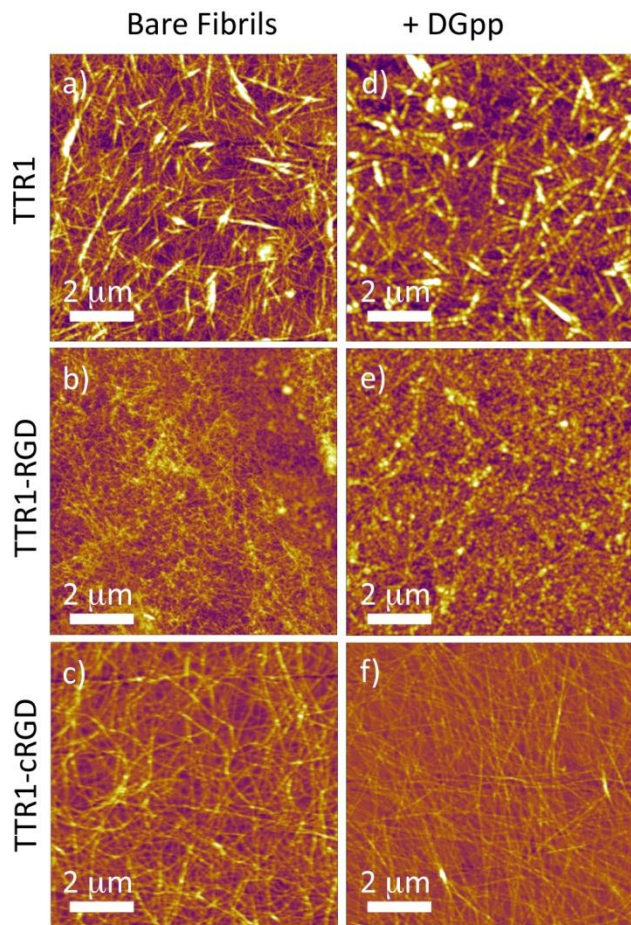


Figure 2: AFM topographic images of TTR1-based fibrils on freshly cleaved mica before (bare fibrils) and after DGpp deposition (+DGpp): the z-scales for TTR1 and TTR1-RGD are 60 nm and for TTR1-cRGD 30 nm. The scale bars are 2  $\mu\text{m}$  in length.

The quantitative effect of depositing the DGpp layer on the nanoscale roughness of the substrates is shown in Figure 3. As observed previously,<sup>1</sup> the TTR1 fibrils showed the highest  $R_{\text{rms}}$  values ( $11.3 \pm 0.58$  nm) at the high surface concentrations examined ( $5 \text{ mgml}^{-1}$ ), followed by the TTR1-RGD fibrils ( $6.6 \pm 0.35$  nm), whilst the TTR1-cRGD surfaces showed considerably lower  $R_{\text{rms}}$  values ( $2.5 \pm 0.28$  nm). Encouragingly, the calculated  $R_{\text{rms}}$  values for the surfaces after DGpp

deposition were statistically indistinguishable from the  $R_{rms}$  values calculated for the bare fibril surfaces ( $10.9 \pm 0.48$  nm,  $7.1 \pm 0.16$  nm and  $1.7 \pm 0.18$  nm for the TTR1-DGpp, TTR1-RGD-DGpp and TTR1-cRGD-DGpp respectively). This result confirms that as previously seen for the fibrils from hen egg white lysozyme,<sup>5</sup> the DGpp coating accurately retains the fibrous nanoscale topography of the amyloid coatings. TTR1, TTR1-RGD and TTR1-cRGD fibrils are known to be hydrophilic with water contact angles between  $10-20^\circ$ .<sup>1</sup> After the deposition of the DGpp film the substrates become more hydrophobic with contact angles  $65 \pm 5^\circ$  for all surfaces.

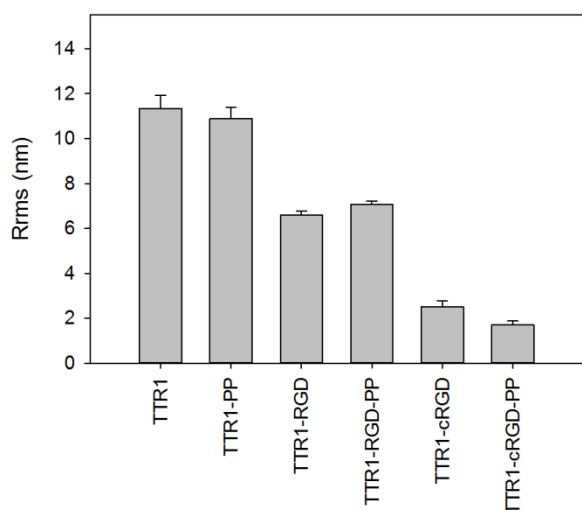


Figure 3: Roughness ( $R_{rms}$ ) measurements calculated from AFM images of bare fibril or fibril and DGpp coated mica surfaces shown in Figure 2. Average values were calculated from at least 3 different images ( $N = 3$ ). Error bars show standard error of mean.

In order to investigate the structural origin of the variation in surface roughness of the three different fibril coatings (Figure 3), higher-magnification AFM images were obtained (Figure 4). The TTR1 fibrils had an average width of  $54.7 \pm 3.0$  nm ( $N = 30$ ), whilst the TTR1-RGD and

TTR1-cRGD fibrils had average widths of  $33.2 \pm 2.0$  nm and  $45.3 \pm 1.1$  nm respectively (N = 30) (Figure S3).

The morphology of the fibrils in the high-magnification AFM images indicates the source of the different  $R_{rms}$  values for the surfaces. Bundles of TTR fibrils are visible in Figure 4a, consisting of many closely interacting sometimes twisting mature TTR1 fibrils. The largest of these formed needle shaped bundles (more clearly seen in the lower resolution AFM images, Figures 2a and 2d). These needle shaped assemblies are considerably larger than the other fibrils seen for the TTR1-RGD or TTR1-cRGD coated surfaces and are likely the structural origin of the higher  $R_{rms}$  values seen for TTR1 fibrils.

The TTR1-RGD coatings (Figure 4b) contained twisted multi-filamentous structures, however, no needle-like assemblies, explaining the reduction in  $R_{rms}$ . In contrast, TTR1-cRGD fibrils in Figure 4c appear smooth and less twisted with little variation in diameter, accounting for the lowest  $R_{rms}$ . The fibril widths measured here are slightly larger but of the same order of magnitude as the widths measured for individual fibrils by cryo-TEM by Biongiiovanni *et. al.*<sup>1</sup>

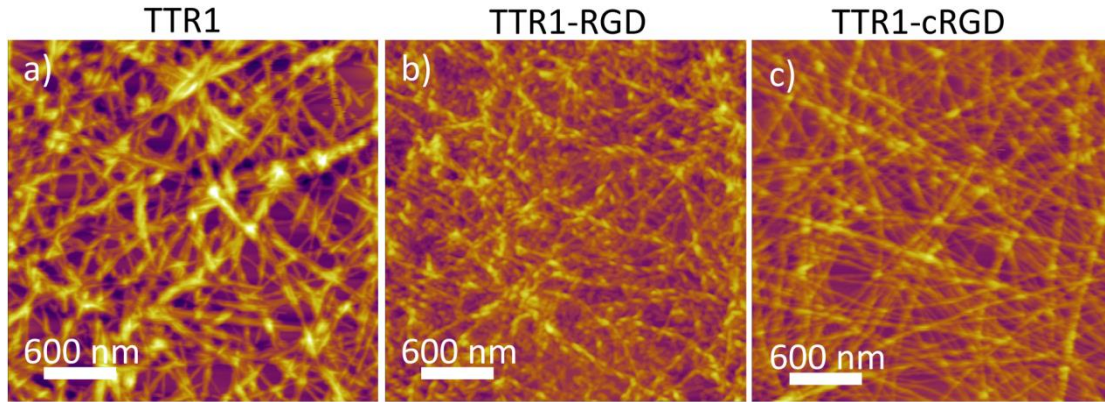


Figure 4: Higher magnification AFM images of the bare amyloid fibril networks: the z-scales for TTR1 and TTR1-RGD are 60 nm and for TTR1-cRGD are 30 nm. The scale bars are 600 nm in length.

### **Cellular Response to Fibril Chemistry and Topography**

To investigate the effects of TTR1-based fibril chemistry and topography versus topography alone, epithelial cells (MA-104) were cultured on each of the TTR1-based fibril coated surfaces or on fibril and DGpp coated surfaces, where the topography differs but the DGpp chemistry is identical. Cells were cultured for 18 h to allow attachment and spreading. Calcein was used to assess viability, as this compound is converted by metabolically active cells and stains the cytoplasm green. Non-viable cells were identified by red fluorescence from ethidium homodimer that accumulates in the nucleus of the cell.

All six substrates coated with bare fibrils or fibrils and a DGpp film supported cell attachment (Figure 5) and a high proportion of the cells observed were metabolically active (Figure 5 c.f. Figure S4, where non-viable cells are shown on the same surfaces).

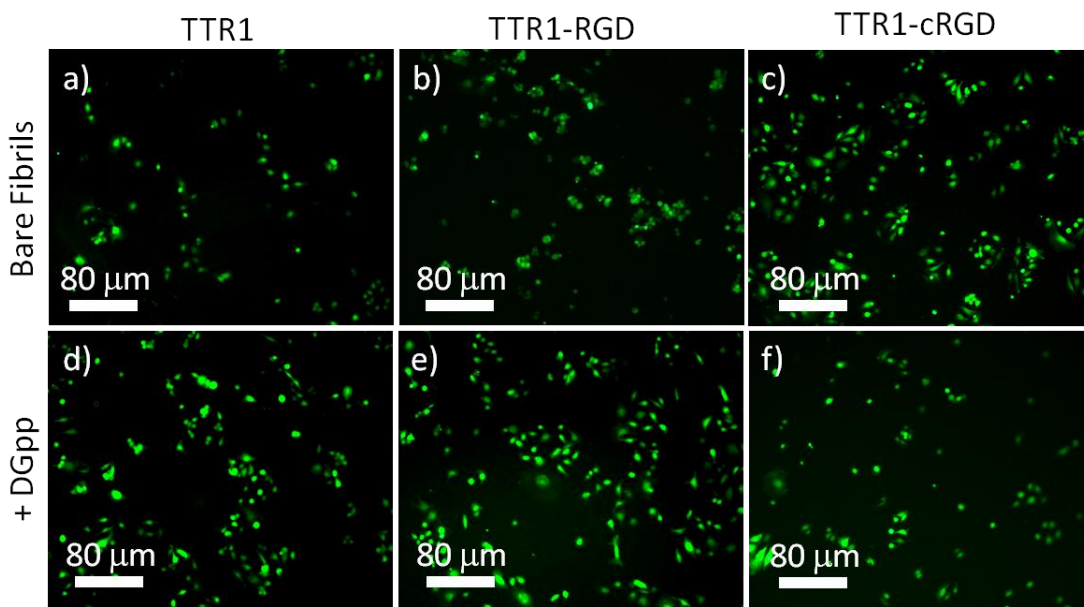


Figure 5: Representative fluorescent microscopy images of metabolically active cells stained with calcein, which appears green. Cells were cultured for 18 h on TTR1-based fibril coated surfaces both with and without a deposited DGpp film. The scale bars are 80 μm in length.

None of the bare fibril or fibril + DGpp coated surfaces induced high levels of toxicity and the number of non-viable cells (expressed as a percentage of total cell number attached to the substrates after washing) was below 10 %. Interestingly, the number of non-viable cells was subtly, but statistically significantly, higher for surfaces coated with TTR1-RGD fibrils ( $8.02 \pm 1.12$  % non-viable) or TTR1-cRGD fibrils ( $7.22 \pm 0.70$  %) compared to TTR1 fibrils ( $4.89 \pm$

1.08 %). The relative toxicities of the TTR1-based fibril coated surfaces without the DGpp layer can be described by the trend TTR1-RGD ~ TTR1-cRGD > TTR.

The same trends in cell viability were observed for cells exposed to DGpp coated substrates (TTR1-RGD-DGpp ~ TTR1-cRGD-DGpp > TTR-DGpp) with TTR1-DGpp =  $2.69 \pm 0.39$  % non-viable, TTR1-RGD-DGpp =  $6.08 \pm 1.04$  % and TTR1-cRGD-DGpp =  $5.51 \pm 0.79$  %. This indicates that surface chemistry was not a major factor in the responses observed and that the underlying differences in topography still present in the DGpp coated surfaces may contribute to the cell response.

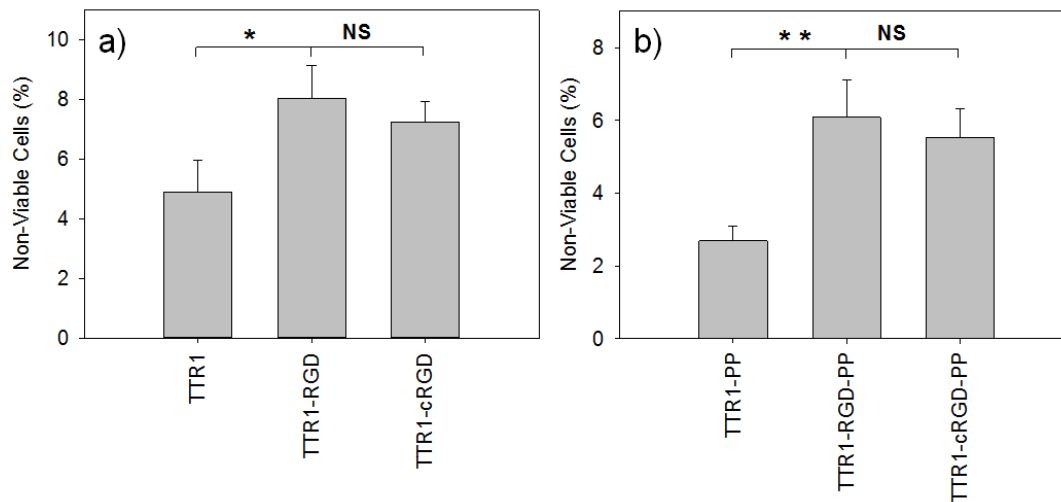


Figure 6: Non viable cells expressed as a percentage of the total number of cells adhered to the surface after washing on a) bare TTR1-based fibril coated surfaces and b) TTR1-based fibril coated surfaces after deposition of a DGpp film. Non-viable cells were detected with ethidium homodimer and viable cells with calcein. Mean values calculated from the data from three

individual experiments (N=3). \* P < 0.05, \*\* P < 0.01, NS = not significant. Error bars show the standard error of the mean.

In the absence of the DGpp film the ability of the TTR1-based fibril coated surfaces to support cell attachment followed the order TTR1-cRGD > TTR1 ~ TTR1-RGD as assessed by the number of metabolically active cells relative to a bare mica surface (Figure 7a). Significantly more cells were attached to the TTR1-cRGD fibril coated surfaces than mica ( $1.90 \pm 0.18$ ) and similar numbers of cells for TTR1 ( $1.1 \pm 0.073$ ) or TTR1-RGD ( $0.99 \pm 0.13$ ) fibril coated surfaces and bare mica.

As was expected from the findings of Reynolds *et. al.*<sup>5</sup>, there was a significant increase in the number of cells attached to the fibril and DGpp coated surfaces compared to bare mica but no significant difference was observed between the three DGpp coated surfaces (Figure 7b) (TTR1-DGpp =  $1.48 \pm 0.25$ , TTR1-RGD-DGpp =  $1.47 \pm 0.25$  or TTR1-cRGD-DGpp =  $1.28 \pm 0.15$  or TTR1-DGpp ~ TTR1-RGD-DGpp ~ TTR1-cRGD-DGpp), indicating that the DGpp coating had effectively masked the cell adhesion ligands removing the chemical differences between the fibril surfaces. A comparison between the number of attached cells on the fibril coatings before and after DGpp deposition revealed a slight increase in the number of cells adsorbed to the DGpp coated substrates, however, this was only significant for the TTR1-RGD fibrils (P\* = 0.04).

Metabolically active cells were most spread on TTR1-cRGD fibril coated surfaces ( $775 \pm 66 \mu\text{m}^2$ ), followed by TTR1 ( $636 \pm 37 \mu\text{m}^2$ ) and TTR1-RGD ( $413 \pm 18 \mu\text{m}^2$ ) (Figure 7c; i.e. TTR1-cRGD > TTR1 > TTR1-RGD). This observation is consistent with previous studies, where the cRGD ligand has been found to be more effective than the RGD ligand at promoting cell spreading on fibrils.<sup>1</sup>

The addition of the DGpp layer altered cell spreading on some fibril coated surfaces, indicating that the fibril surface chemistry is important for cell spreading, although topography may also contribute for some surfaces. Cells on the TTR1-cRGD-DGpp coated surface spread to a similar extent as observed on TTR1-RGD-DGpp coated surfaces ( $588 \pm 69 \mu\text{m}^2$ ) (Figure 7d; i.e. TTR1-DGpp > TTR1-RGD-DGpp ~ TTR1-cRGD-DGpp), indicating these surfaces were now less favourable for cell spreading. Cells were significantly more spread on the TTR1-DGpp coated surface relative to the TTR1-RGD-DGpp coated surface ( $682 \pm 66 \mu\text{m}^2$  and  $559 \pm 38 \mu\text{m}^2$  respectively), similar to observations for the uncoated surfaces, suggesting that the topographic differences may be more important than differences in surface chemistry for these two surfaces. A comparison of the area of cells on the DGpp coated and bare fibril coated surfaces reveals no significant increase in cell spreading on the DGpp coated substrates, except for TTR1-RGD fibril vs TTR1-RGD-DGpp coated surfaces ( $P^{**} = 0.04$ ).

These results taken together show that surface chemistry determines the number of viable cells that attach on TTR1-based fibril coated surfaces, while the topography influences the number of non-viable cells. Cell spreading, however, can be influenced by both the surface chemistry and topography of TTR1-based fibrils, these effects are summarized in Table 1.

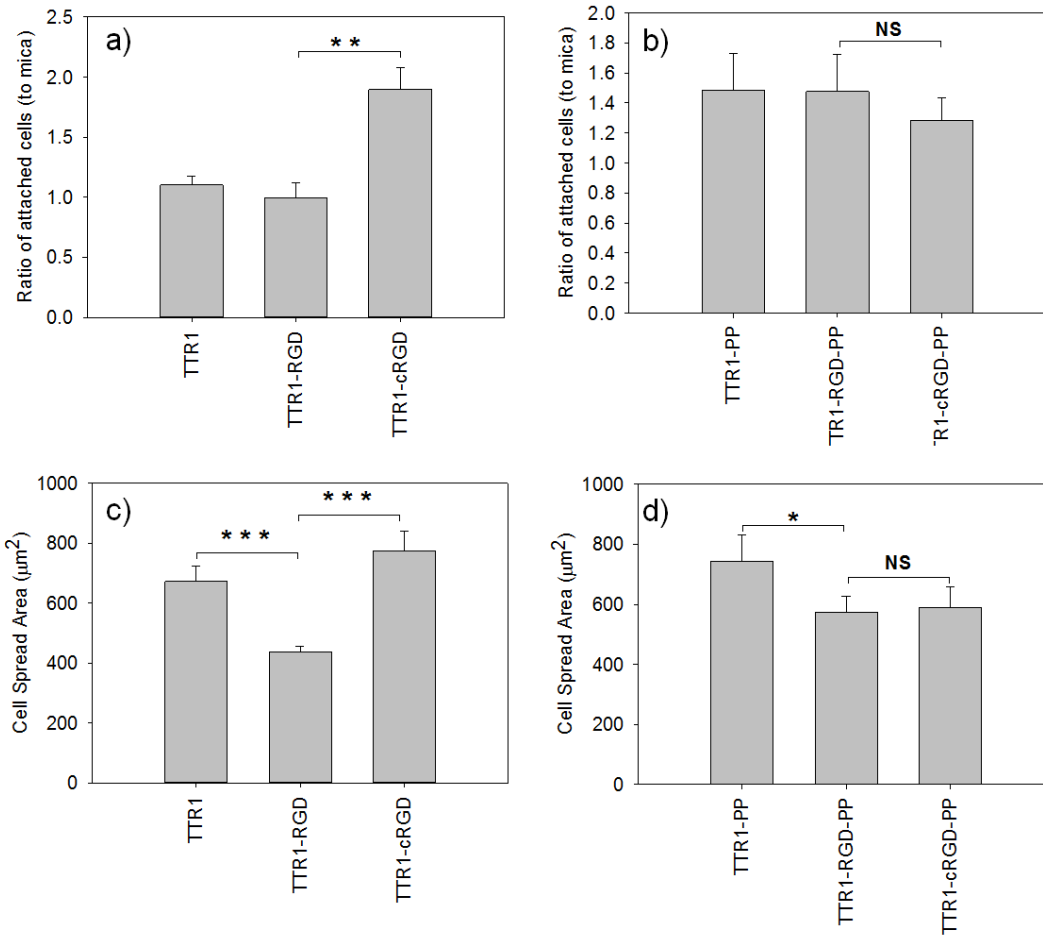


Figure 7: a-b) Number of metabolically active cells measured with calcein after 18 h in cell culture. The number of cells adsorbed is expressed as a ratio of the number on a freshly cleaved mica substrate. Treatments were a) bare TTR-1 based fibril coated surfaces and b) TTR1-based fibril coated surfaces after deposition of a DGpp film. c-d) Mean spread area of cells cultured for 18 h on either c) bare TTR-1 based fibril coated surfaces or d) TTR-1 fibril coated surfaces after deposition of a DGpp film. Mean values were calculated from the data from three individual experiments (N=3) \*  $P < 0.05$ , \*\*  $P < 0.01$ , \*\*\*  $P < 0.001$  NS = not significant. Error bars show the standard error of mean.

Table 1: Overview of cellular responses to fibril chemical and topographic effects. Examples where trends differ due to the DGpp coating are highlighted in red.

	Cell Viability	Cell Attachment	Cell Spreading
Fibril chemical and topographic effects (bare fibril coated surfaces)	TTR1-RGD ~ TTR1-cRGD > TTR1	TTR1-cRGD > TTR1 ~ TTR1-RGD	TTR1-cRGD > TTR1 > TTR1-RGD
Fibril topographic effects only (fibril +DGpp coated surfaces)	TTR1-RGD ~ TTR1-cRGD > TTR1	TTR1-cRGD ~ TTR1 ~ TTR1-RGD	TTR1 > TTR1-RGD ~ TTR1-cRGD
Chemical or topographic effect	Topographic effect	Chemical effect	Both chemical and topographic effect

Next, the ability of metabolically active cells to make strong adhesive contacts with the substrate, known as focal adhesions (FA), was determined by immunofluorescence using an Alexa-488 phalloidin probe for F-actin and Alexa-594 probe for vinculin. These intracellular proteins indicate cytoskeletal development and stress fiber formation within the cell and the formation of integrin mediated FA with the underlying matrix<sup>29</sup> respectively. FA's play important physiological roles in controlling cell shape, mechanotransduction and signal transduction.<sup>29-31</sup>

The alexa-488 phalloidin stained images indicate some degree of cytoskeletal formation and stress fiber formation for all three of the bare fibril coated surfaces but these stress fibers are

longer and more aligned within cells on the TTR1-cRGD fibril coated surfaces. FA's are evident in the cells adherent on the TTR1-based fibril coated surfaces, as seen by small punctuate spots shown by the vinculin stain. The FAs formed on the TTR1-cRGD networks are more distinct and larger than occurs in the cells on the TTR1-RGD or TTR1 fibril coated surfaces and these FA are located at the ends of stress fibers.

Cell stress fibers and FA's were present to a similar extent in cells on each of the three surfaces following deposition of the DGpp layer. The DGpp layer is known to encourage serum protein adsorption and provide a favourable surface for cell attachment.<sup>5,24,26</sup>

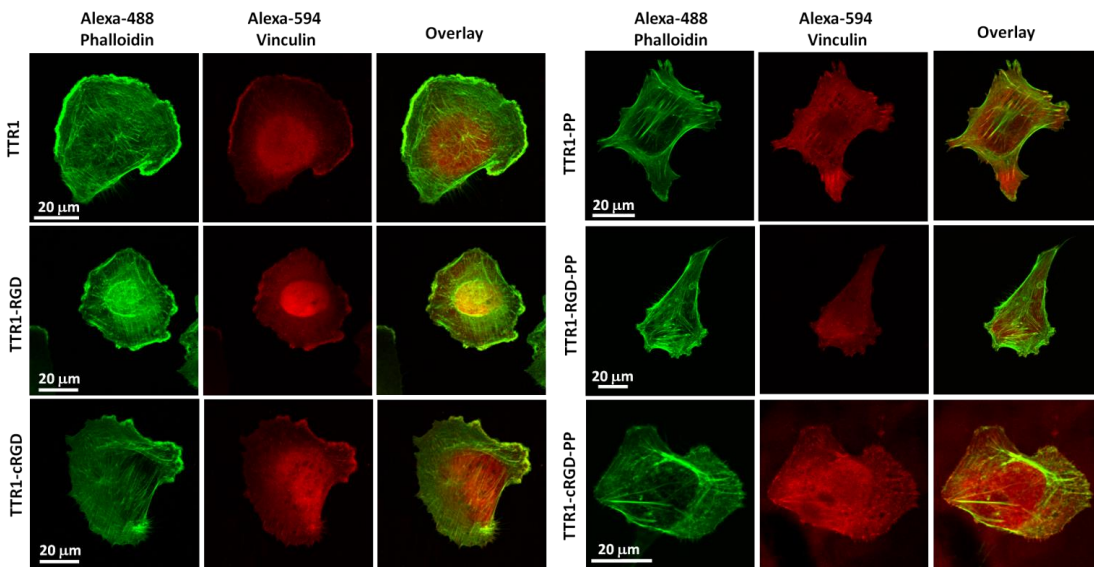


Figure 8: Representative confocal microscopy images of cells cultured for 18 h on the bare TTR1-based fibril coated surfaces (left) or fibril and DGpp coated surfaces (right). The alexa-488 phalloidin stain shown in green (left columns) indicates cytoskeletal development, while the alexa-594 vinculin stain shown in red (centre) shows the development of integrin mediated focal

adhesions between the cell membrane and the surface. The right hand columns show an overlay of the two images from the left and centre columns. The scale bars are all 20  $\mu\text{m}$  in length.

The combined results of the cell culture experiments show that both the surface chemistry of fibrils and topography of fibril coated surfaces can influence interactions with cells. Fibril chemistry, such as the cyclised RGDfK ligand, is known to promote cell attachment and spreading but this effect is masked by the DGpp layer. The topography was also found to control cell viability and to also alter cell spreading.

## **Discussion**

As previously observed by Reynolds *et. al.*<sup>5</sup> the deposition of plasma polymer films onto amyloid fibril coatings represents a convenient method of masking the underlying surface chemistry of the amyloid network, whilst accurately retaining the nanoscale fibrous topography. The previous study acted as a proof-of-principle experiment to show the validity of the method and here we use the DGpp coating to mask the effects of surface chemical effects for a variety of amyloid fibrils assembled from peptide fragments based on the TTR protein. This enabled us to deconvolute the combined topographical and chemical effects of the biomimetic amyloid fibril coated surfaces on cultured mammalian cells.

AFM images revealed subtle differences in topography for each of the fibril coated surfaces (TTR1 vs. TTR1-RGD vs. TTR1-cRGD). Following DGpp coating each surface looked quantitatively similar to the bare fibril coated surfaces with no significant differences in rms

roughness caused by the addition of the DGpp film (TTR1 vs. TTR1-DGpp, TTR1-RGD vs TTR1-RGD-DGpp). Hence, as previously seen for the fibrils from hen egg white lysozyme, the DGpp coating accurately retains the fibrillar nanoscale topography of the amyloid fibril coatings.<sup>5</sup> As the same deposition conditions and also the same underlying substrate (mica) was used as in Reynolds *et. al.*<sup>5</sup> it can also be assumed that the DGpp films were of a comparable thickness (approx. 150 nm) and successfully masked the surface chemistry of the underlying fibrils.

All three TTR-1 based peptides form multi-filamentous assemblies. This can be seen in the AFM images in Figure 4 and in the difference between the measured fibril widths and the ~4 nm in width determined for protofilaments formed by the TTR<sub>105-115</sub> fragment calculated by Debelouchina *et. al.*<sup>11</sup> TTR1 fibrils formed large needle like bundles, TTR1-RGD fibrils smaller twisted ribbon like structures containing multiple filaments and TTR1-cRGD more uniform fibrils with a narrower distribution of measured widths. One explanation for the morphology of TTR1-cRGD fibrils could be the partial closure of the multi-stranded ribbons into nanotubes, as observed for fibrils from hen egg white lysozyme.<sup>32</sup>

Previous research has shown that the cross- $\beta$  core structure adopted by TTR1 and sequence variants based on TTR1 such as TTR1-RGD fibrils is identical.<sup>21</sup> The change in fibril morphology arises from non-core residues that impose different packing constraints on the protofilaments when they assemble into multi-filamentous structures. The current study therefore

provides further evidence that both the sequence and environmental conditions can have a significant effect on the morphologies of fibrils.<sup>33-35</sup>

The toxicity of TTR1-RGD and TTR1-cRGD fibrils is likely due to small changes in the topography of these fibrils, as an increase in non-viable cells was observed for surfaces coated in these fibrils regardless of the presence of the DGpp film (which acts to mask the fibril chemistry). This indicates that irrespective of any chemical functionalization of the substrates, the nanoscale topography of the RGD and cRGD fibrils had statistically significant negative effect on the viability of cultured epithelial cells.

We speculate that the origin of the increased toxicity for the TTR1-RGD and TTR1-cRGD fibril networks arises from the shearing action of exposed toxic fibril ends on the cell membrane. Recent research showed that the cytotoxicity of TTR1 based fibrils is due to cell membrane damage, which triggers an apoptotic response<sup>28</sup> and there is increasing evidence that fibrils, or pre-fibrillar aggregates, damage the cell membrane.<sup>13,36,37</sup> Amyloid fibrils have also been observed to damage the membrane of lipid vesicles by a shearing action of the fibril ends, which removes lipids from the membrane.<sup>38</sup>

The toxic ends of TTR1-cRGD and TTR1-RGD fibrils may extend from a heterogeneous fibril coated surface. The majority of the surface presented could be compatible and presents the RGD or cRGD ligand to the cell but at other points the exposed fibril ends could result in membrane

damage and cell death. It is interesting to note that no increase in cytotoxicity was observed for the TTR1-cRGD fibrils in Bongiovanni *et. al.*<sup>1</sup>, where much higher concentrations of surface bound fibrils were used to ensure complete coverage. This higher coverage may have created a more homogeneous surface where the fibril ends are masked and the toxic response reduced. The AFM images taken at high concentrations of fibrils (2.5 mgml<sup>-1</sup>) in figure S1 support this hypothesis, as it is difficult to resolve the individual fibrils within these images. Fibril aggregation may also explain the drop in toxicity for the TTR1 fibrils; here the toxic fibril ends maybe hidden by the large needle like bundles formed.

The adhesive chemistry and physiological orientation of the cRGD groups on the fibril surface appears to have a greater effect than the negative topographical influence of the fibrils as cell attachment and spreading was improved on the TTR1-cRGD fibrils compared to the TTR1 and TTR1-RGD fibrils only in the absence of the DGpp film. As previously seen<sup>1</sup> for cells cultured on TTR1-cRGD substrates the FAs generated are larger and more distinct compared to the linear RGD or non-functionalized fibrils and the actin stress fibers present appear more aligned and cross the cell body, indicative of strong mechano-transduction effects between integrins in the cell membrane and the cRGD ligands decorating the fibrils.<sup>39</sup>

Fibril topography appears to play an important role in cell attachment and spreading, as it does with cell viability. Cell attachment and spreading on the TTR1 and TTR1-RGD substrates appear to show a similar trend either with or without the DGpp layer. Little change in the relative

affinities for cell attachment is seen for TTR1 vs. TTR1-RGD following DGpp coating and cells are less spread on TTR1-RGD surfaces than TTR1 surfaces in the absence or presence of DGpp.

Cell attachment and spreading may be aided by adsorption of serum proteins such as such as Fibronectin, (Fn) or collagen from the cell culture media onto the fibril surfaces. The higher rms roughness values for the TTR1 substrates will increase the surface area available for protein adsorption. The nanotopographic features of the fibril coated surfaces could also protect the adsorbed serum proteins from denaturation,<sup>5,40</sup> promoting further attachment and spreading. The concentration of protein adsorption is expected to be relatively low; however, due to the proteinaceous and hydrophilic nature of amyloid fibrils.<sup>1,5</sup> This low level of adsorbed proteins likely explains the marked improvement in cell attachment and spreading on cycloRGDfK fibril coated surfaces.

Stress fiber and FA formation was more marked on TTR1 or TTR1-RGD fibril coated surfaces observed here than for the same cells in a prior study by Bongoivanni *et al.*,<sup>1</sup> as the cells were incubated for a much longer period of 18 h compared to 1 h for the previous study focusing on the initial stages of cell attachment. The longer incubation employed here allows sufficient time for a layer of adhesive proteins to adsorb to the interface via the Vroman effect.<sup>41</sup> This layer of proteins will promote FA and stress fiber formation in the absence of cell adhesive chemistries on fibril surfaces.

The presence of distinct stress fibers and FAs on all networks after DGpp deposition is likely due to the surface chemistry of the DGpp. Under the deposition conditions used here, the surfaces contain a high concentration of un-substituted hydrocarbon polymer chains<sup>5,24,26</sup> Resulting in a surface more hydrophobic than either the mica control or the bare fibrils, thus encouraging serum protein adsorption<sup>5</sup> resulting in a favourable surface for attaching cells.<sup>24</sup>

In this work we concentrate on using the DGpp films as a tool to allow us to deconvolute the effects of surface topography and chemistry on cultured cells. A possible alternative application of the nanotopographic DGpp films would be for use as potential biomaterials to promote or control cell attachment.<sup>5</sup> Statistical analysis comparing the viability of cells on bare fibrils and those coated with the DGpp layer, however, revealed no significant reduction in cytotoxicity for any of the TTR1 based fibril systems investigated with DGpp deposition. Cell attachment and spreading were also not significantly improved by DGpp film deposition on TTR1 or TTR1-cRGD fibrils and only moderately improved for TTR1-RGD fibrils. We therefore conclude that for this system the presence of the DGpp layer offers little benefit for biomaterial applications looking to improve or control cellular attachment and spreading.

By deconvoluting the effects of surface chemistry and surface topography we have shown that both significantly influence the viability and attachment of epithelial cells cultured on TTR1-based amyloid fibrils. This method may also aid the design of biomaterials or fundamental research into structure-function relationships of amyloid fibrils. An example of the former is the development of materials with nanoscale topographies to control stem-cell phenotypes<sup>16</sup> and for

the latter mutations to the non-core residues of PMEL amyloid fibrils, which have been shown to convert the fibrils from a functional to a pathological form.<sup>42</sup> The DGpp method could therefore be used to investigate if a change in amyloid topography underpins a change in toxicity.

## **Conclusions**

Through the application of a reductionist approach using a plasma polymer film deposited on a range of TTR1-based fibril coated surfaces, we have deconvoluted the effects of cell adhesive surface chemistry and topography. Our results demonstrate that both topography and biomimetic surface chemistries play important roles in controlling the viability, attachment and spreading of epithelial cells. This study highlights the importance of carefully considering nanoscale topography and chemistry when rationally designing novel biomaterials. DGpp deposition can also be used to give insights into the relative roles of topography and chemistry in both functional amyloid fibrils and those connected to neurodegenerative diseases.

**Supporting Information.** The following Supporting Information is available: AFM images of TTR1 fibrils on mica at a range of concentrations, AFM images of TTR1+ DGpp films after hydration (18 h); graphical representation of the quantification of TTR fibril widths from AFM data; and representative images of ethidium homodimer stained cells on all TTR functionalized surfaces (with and without DGpp). This material is available free of charge via the Internet at <http://pubs.acs.org>.

AUTHOR INFORMATION

## Corresponding Authors

\*Nicholas P Reynolds email: [nick.reynolds@csiro.au](mailto:nick.reynolds@csiro.au) and Sally L. Gras email

[sgras@unimelb.edu.au](mailto:sgras@unimelb.edu.au)

## Author Contributions

The manuscript was written through contributions of all authors. All authors have given approval to the final version of the manuscript.

## Acknowledgements

Peptide synthesis of the TTR1-cycloRGDfK peptide was carried out by John Karas in the Peptide Technology Facility of the Bio21 Molecular Science and Biotechnology Institute, The University of Melbourne. NPR acknowledges a personal fellowship from the Swiss National Science Foundation (SNSF) (PBSKP2\_145829). SLG is supported by the ARC Dairy Innovation Hub (IH120100005).

## References

- (1) Bongiovanni, M. N.; Scanlon, D. B.; Gras, S. L. *Biomaterials* **2011**, *32*, 6099.
- (2) Mata, A.; Hsu, L.; Capito, R.; Aparicio, C.; Henrikson, K.; Stupp, S. I. *Soft Matter* **2009**, *5*, 1228.
- (3) Silva, G. A.; Czeisler, C.; Niece, K. L.; Beniash, E.; Harrington, D. A.; Kessler, J. A.; Stupp, S. I. *Science* **2004**, *303*, 1352.
- (4) Reynolds, N. P.; Charnley, M.; Mezzenga, R.; Hartley, P. G. *Biomacromolecules* **2014**, *15*, 599.
- (5) Reynolds, N. P.; Styan, K. E.; Easton, C. D.; Li, Y.; Waddington, L.; Lara, C.; Forsythe, J. S.; Mezzenga, R.; Hartley, P. G.; Muir, B. W. *Biomacromolecules* **2013**, *14*, 2305.
- (6) Li, C.; Adamcik, J.; Mezzenga, R. *Nat. Nanotechnol.* **2012**, *7*, 421.

- (7) Zhong, C.; Gurry, T.; Cheng, A. A.; Downey, J.; Deng, Z.; Stultz, C. M.; Lu, T. K. *Nat. Nanotechnol.* **2014**, *9*, 858.
- (8) Udomprasert, A.; Bongiovanni, M. N.; Sha, R.; Sherman, W. B.; Wang, T.; Arora, P. S.; Canary, J. W.; Gras, S. L.; Seeman, N. C. *Nat. Nanotechnol.* **2014**, *9*, 537.
- (9) Conway, K. A.; Lee, S. J.; Rochet, J. C.; Ding, T. T.; Williamson, R. E.; Lansbury, P. T. *Proc. Natl. Acad. Sci. U. S. A.* **2000**, *97*, 571.
- (10) Winner, B.; Jappelli, R.; Maji, S. K.; Desplats, P. A.; Boyer, L.; Aigner, S.; Hetzer, C.; Loher, T.; Vilar, M.; Campionic, S.; Tzitzilonis, C.; Soragni, A.; Jessberger, S.; Mira, H.; Consiglio, A.; Pham, E.; Masliah, E.; Gage, F. H.; Riek, R. *Proc. Natl. Acad. Sci. U. S. A.* **2011**, *108*, 4194.
- (11) Debelouchina, G. T.; Bayro, M. J.; Fitzpatrick, A. W.; Ladizhansky, V.; Colvin, M. T.; Caporini, M. A.; Jaroniec, C. P.; Bajaj, V. S.; Rosay, M.; MacPhee, C. E.; Vendruscolo, M.; Maas, W. E.; Dobson, C. M.; Griffin, R. G. *J. Am. Chem. Soc.* **2013**, *135*, 19237.
- (12) Rabe, M.; Soragni, A.; Reynolds, N. P.; Verdes, D.; Liverani, E.; Riek, R.; Seeger, S. *ACS Chem. Neurosci.* **2013**, *4*, 408.
- (13) Reynolds, N. P.; Soragni, A.; Rabe, M.; Verdes, D.; Liverani, E.; Handschin, S.; Riek, R.; Seeger, S. *J. Am. Chem. Soc.* **2011**, *133*, 19366.
- (14) Fowler, D. M.; Koulov, A. V.; Balch, W. E.; Kelly, J. W. *Trends Biochem. Sci.* **2007**, *32*, 217.
- (15) Bosman, F. T.; Stamenkovic, I. *J. Pathol.* **2003**, *200*, 423.
- (16) Turner, L.-A.; J. Dalby, M. *Biomater. Sci.* **2014**, *10.1039/C4BM00155A*
- (17) Luna, J. I.; Ciriza, J.; Garcia-Ojeda, M. E.; Kong, M.; Herren, A.; Lieu, D. K.; Li, R. A.; Fowlkes, C. C.; Khine, M.; McCloskey, K. E. *Tissue Eng., Part C* **2011**, *17*, 579.
- (18) Wang, L.; Murthy, S. K.; Fowle, W. H.; Barabino, G. A.; Carrier, R. L. *Biomaterials* **2009**, *30*, 6825.
- (19) Cardoso, I.; Goldsbury, C. S.; Muller, S. A.; Olivieri, V.; Wirtz, S.; Damas, A. M.; Aebi, U.; Saraiva, M. J. *J. Mol. Biol.* **2002**, *317*, 683.
- (20) Deng, W.; Cao, A. N.; Lai, L. H. *Biochem. Biophys. Res. Commun.* **2007**, *362*, 689.
- (21) Bongiovanni, M. N.; Puri, D.; Goldie, K. N.; Gras, S. L. *J. Mol. Biol.* **2012**, *421*, 256.
- (22) Bongiovanni, M. N.; Caruso, F.; Gras, S. L. *Soft Matter* **2013**, *9*, 3315.

- (23) Gras, S. L. *Aust. J. Chem.* **2007**, *60*, 333.
- (24) Menzies, D. J.; Jasieniak, M.; Griesser, H. J.; Forsythe, J. S.; Johnson, G.; McFarland, G. A.; Muir, B. W. *Surf. Sci.* **2012**, *606*, 1798.
- (25) Menzies, D. J.; Nelson, A.; Shen, H.-H.; McLean, K. M.; Forsythe, J. S.; Gengenbach, T.; Fong, C.; Muir, B. W. *J. R. Soc., Interface* **2012**, *9*, 1008.
- (26) Muir, B. W.; Tarasova, A.; Gengenbach, T. R.; Menzies, D. J.; Meagher, L.; Rovere, F.; Fairbrother, A.; McLean, K. M.; Hartley, P. G. *Langmuir* **2008**, *24*, 3828.
- (27) Gras, S. L.; Tickler, A. K.; Squires, A. M.; Devlin, G. L.; Horton, M. A.; Dobson, C. M.; MacPhee, C. E. *Biomaterials* **2008**, *29*, 1553.
- (28) Bongiovanni, M. N.; Gras, S. L. *Biomaterials* **2015**, *46*, 105.
- (29) Geiger, B.; Bershadsky, A.; Pankov, R.; Yamada, K. M. *Nat. Rev. Mol. Cell Biol.* **2001**, *2*, 793.
- (30) Vogel, V.; Sheetz, M. *Nat. Rev. Mol. Cell Biol.* **2006**, *7*, 265.
- (31) Geiger, B.; Spatz, J. P.; Bershadsky, A. D. *Nat. Rev. Mol. Cell Biol.* **2009**, *10*, 21.
- (32) Lara, C.; Handschin, S.; Mezzenga, R. *Nanoscale* **2013**, *5*, 7197.
- (33) Usov, I.; Adamcik, J.; Mezzenga, R. *ACS Nano* **2013**, *7*, 10465.
- (34) Usov, I.; Adamcik, J.; Mezzenga, R. *Faraday Discuss.* **2013**.
- (35) Lara, C.; Reynolds, N. P.; Berryman, J. T.; Zhang, A.; Xu, A.; Mezzenga, R. *J. Am. Chem. Soc.* **2014**, *136*, 4732.
- (36) Domanov, Y. A.; Kinnunen, P. K. J. *J. Mol. Biol.* **2008**, *376*, 42.
- (37) Robinson, P. J.; Pinheiro, T. J. T. *Biophys. J.* **2010**, *98*, 1520.
- (38) Milanesi, L.; Sheynis, T.; Xue, W.-F.; Orlova, E. V.; Hellewell, A. L.; Jelinek, R.; Hewitt, E. W.; Radford, S. E.; Saibil, H. R. *Proc. Natl. Acad. Sci. U. S. A.* **2012**, *109*, 20455.
- (39) Tojkander, S.; Gateva, G.; Lappalainen, P. *J. Cell Sci.* **2012**, *125*, 1855.
- (40) Elter, P.; Weihe, T.; Buehler, S.; Gimsa, J.; Beck, U. *Colloids Surf., B* **2012**, *95*, 82.
- (41) Vroman, L.; Adams, A. L.; Fischer, G. C.; Munoz, P. C. *Blood* **1980**, *55*, 156.
- (42) Watt, B.; Tenza, D.; Lemmon, M. A.; Kerje, S.; Raposo, G.; Andersson, L.; Marks, M. S. *PLoS Genet.* **2011**, *7*.

**ToC Image**

